Local properties of extended self-similarity in three-dimensional turbulence

Daigen Fukayama,[1] Tohru Nakano,[1] Alexander Bershadskii,[1,2] and Toshiyuki Gotoh[3]
[1]*Department of Physics, Chuo University, Tokyo 112-8551, Japan*
[2]*Machanaim Center, P.O. Box 31155, Jerusalem 91000, Israel*
[3]*Department of Systems Engineering, Nagoya Institute of Technology, Nagoya 466-8555, Japan*
(Received 21 June 2000; published 14 June 2001)

Using a generalization of extended self-similarity we have studied local scaling properties of incompressible homogeneous isotropic three-dimensional turbulence in a direct numerical simulation. We have found that these properties are consistent with log-normal-like behavior of the velocity increments with moderate amplitudes for space scales r beginning from Kolmogorov length η up to the largest scales, and in the whole range of the Reynolds numbers: $50 \leqslant R_\lambda \leqslant 459$. The locally determined intermittency exponent $\mu(r)$ varies with r; it has a maximum at scale $r = 14\eta$, independent of R_λ.

DOI: 10.1103/PhysRevE.64.016304 PACS number(s): 47.27.Ak, 05.20.Jj, 47.27.Gs, 47.27.Jv

So-called extended self-similarity (ESS) in incompressible turbulent flows is intensively studied in recent years (see, for instance, [1–8] and references therein). The ESS implies scaling relation between moments of different order. For example, for absolute value of longitudinal velocity increments over separation r in the inertial range the ESS means

$$\langle u_r^q \rangle \sim \langle u_r^p \rangle^{\rho(q)/\rho(p)}, \tag{1}$$

where the scaling exponent $\rho(q)$ is some function of q. It is shown in numerous experiments and numerical simulations that the range of applicability of the ESS is substantially larger than that for ordinary self-similarity, and the ESS can exist even for situations where the ordinary self-similarity cannot be observed at all.

The aim of the present paper is twofold. The first is to study local properties of ESS defined as

$$\langle u_r^p \rangle \sim \langle u_r^3 \rangle^{\zeta_p(r)}, \tag{2}$$

where $\zeta_p(r)$ are depending on r. The local approach allows to develop some old ideas. At past a representation $\zeta_p = p/3 - \mu p(p-3)/18$ derived from a log-normal model, was shown to hold for the values averaged over an inertial interval of certain extension. Here we will show that the representation holds locally (i.e., with $\zeta_p(r)$ and $\mu(r)$ depending on r) in the above defined sense, ranging from the dissipative Kolmogorov length η to integral scale for any observed Reynolds number in direct numerical simulations up to $R_\lambda = 459$.

The second aim is to examine the implication of the variation of the local intermittency exponent $\mu(r)$. It is often mentioned that there is no characteristic length in turbulence, so that the structure functions obey a power law in the inertial region and the associated scaling exponents are independent of scale. However, a recent study of turbulence reveals the existence of the structures [9]. A question, then, naturally arises as to whether there may be any characteristic length ascribed to the structures [10]. The peculiar variation of $\mu(r)$ with respect to r, observed in the paper, indicates that there is a certain length affecting the ESS.

The She-Leveque model [11] is also very popular in the last years. For this model the local exponent is expressed in a general form,

$$\zeta_p(r) = \frac{p}{3}(1-\gamma) + \frac{\gamma}{1-\beta}[1-\beta^{p/3}], \tag{3}$$

where β and γ can be also supposed to depend on r; $\beta(r)$ and $\gamma(r)$ could be, in principle evaluated by plotting the local exponent $\zeta_p(r)$ against p with r fixed. Since here we focus the lower order structure functions that are computed more reliably than the higher order ones, the comparison of the data with the formula is done using a simpler log-normal model with one parameter. If one could compute the higher order structure functions, the comparison should be made with the She-Leveque model.

Let us begin with the derivation of useful formulas on the basis of the log-normal distribution of the dissipation rate ε_r averaged over spheres of radius r,

$$P(\varepsilon_r) = \frac{\varepsilon_r^{-1}}{\sqrt{2\pi\sigma^2}} \exp\left(-\frac{(\ln \varepsilon_r - a)^2}{2\sigma^2} \right), \tag{4}$$

from which we obtain

$$\frac{\langle \varepsilon_r^q \rangle}{\langle \varepsilon_r \rangle^q} = e^{\sigma^2 q(q-1)/2} \tag{5}$$

that results in a parameter-independent type of ESS [1,2] of turbulent energy dissipation

$$\frac{\langle \varepsilon_r^q \rangle}{\langle \varepsilon_r \rangle^q} = \left(\frac{\langle \varepsilon_r^p \rangle}{\langle \varepsilon_r \rangle^p} \right)^{[q(q-1)]/[p(p-1)]}. \tag{6}$$

What is the equivalent relation for the velocity increment? According to the refined similarity method [12–16] $u_r \sim (r\varepsilon_r)^{1/3}$ in the inertial region, while $u_r \sim r\varepsilon_r^{1/2}$ in the dissipative region. If we take regions of scale r between the inertial and dissipative regions, some are described by the former relation, while the others are by the latter one, so that

u_r is related to ε_r in a probabilistic way. For the sake of simplicity we assume a general relation

$$u_r = c(r)\varepsilon_r^{1/\alpha(r)} \tag{7}$$

in a mean sense. Here $\alpha(r)$ is a function of r and coefficient $c(r)$ does not necessarily scale with r. Substituting Eq. (7) into Eq. (6) yields

$$\frac{\langle u_r^q \rangle}{\langle u_r^\alpha \rangle^{q/\alpha}} = \left(\frac{\langle u_r^p \rangle}{\langle u_r^\alpha \rangle^{p/\alpha}} \right)^{[q(q-\alpha)]/[p(p-\alpha)]}. \tag{8}$$

Note that this expresses how the structure functions of different order are related to each other with value of r fixed. This relation can be considered as a functional equation and a solution to this equation is

$$\langle u_r^q \rangle \sim \langle u_r^{\alpha(r)} \rangle^{q/\alpha(r)+b(r)q(q-\alpha(r))}, \tag{9}$$

where $b(r)$ is an arbitrary function of r. Relation (9) is a generalization of ordinary ESS [1,2]. The difference between ordinary ESS and relation (9) is that parameters used in Eq. (9) can depend on r. Therefore we will call this type of ESS as extended *local* self-similarity (ELSS).

To be consistent with the present data processing we express the qth order structure function in terms of the third order structure function as Eq. (2). Making use of Eq. (9), we are led to

$$\zeta_q(r) = \frac{q}{3} - \frac{\mu(r)}{18} q(q-3), \tag{10}$$

where

$$\mu(r) = -\frac{6b(r)\alpha(r)}{1+\alpha(r)[3-\alpha(r)]b(r)}. \tag{11}$$

In the frame of ELSS the exponent ζ_q depends also on r, and below we compare Eqs. (2) and (10) with data of DNS for different values of r. It should be noted that the ELSS expression (10) holds for any value of $\alpha(r)$, so that the expression can be compared with the data for any scale separation without paying attention to which region is being considered.

We have performed a series of direct numerical simulations (DNS's) of incompressible homogeneous isotropic turbulence using a resolution up to 1024^3. Reynolds numbers range from 50 to 459 [18]. The random force is statistically homogeneous, isotropic and Gaussian white, and applied to the band $1 \lesssim k \lesssim 3$ in which the forcing spectrum is constant. The code uses the pseudospectral method and the fourth order Runge-Kutta-Gill one. Initial conditions are Gaussian random velocity fields with the energy spectrum $E(k) \propto k^4 \exp[-2(k/k_0)^2]$, and the resolution is $N=256^3$ for $R_\lambda = 69$, $N=512^3$ for $R_\lambda = 125,176,259$, and $N=1024^3$ for $R_\lambda = 374,459$. After about two eddy turnover times all the turbulent fields attained statistically steady states, which were confirmed by observing the time evolution of the total energy and enstrophy, and the skewness of the longitudinal velocity derivative. For $R_\lambda = 459$ run, the Reynolds number was gradually increased through two steady states. The condition $k_{\max}\eta > 1$ for the resolution of DNS is satisfied for most runs, but that of $R_\lambda = 459$ is slightly less than unity. The statistical averages were taken as the time average over tens of turnover times for lower Reynolds numbers and over a few turnover times for the higher Reynolds numbers; over 45 samples during 2.9 eddy turnover times for $R_\lambda = 374$ and over 31 samples during 1.4 eddy turnover times $R_\lambda = 459$. Computations with $R_\lambda \leqslant 259$ have been done using a vector parallel machine with 16 processors, Fujitsu VPP700E at RIKEN, and those for higher R_λ, using Fujitsu VPP5000/56 with 32 processors at Nagoya University Computation Center.

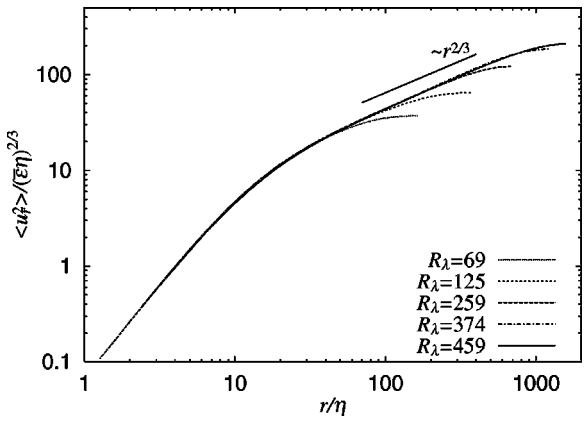

FIG. 1. A plot of $\langle u_r^2 \rangle$ divided by $(\overline{\varepsilon}\eta)^{2/3}$ vs r/η for various values of Reynolds number. An inserted solid line is proportional to $r^{2/3}$. Notice that all data points collapse on a single curve in the dissipative region.

Now turn to the data analysis. Figure 1 is a plot of $\langle u_r^2 \rangle / (\overline{\varepsilon}\eta)^{2/3}$ against r/η for various values of Reynolds number, where $\overline{\varepsilon}$ is the average dissipation rate, and $\eta = (\nu^3/\overline{\varepsilon})^{1/4}$ with molecular viscosity ν. Here a straight solid line proportional to $r^{2/3}$ is inserted. It is remarkable that all data points collapse on a single line in the dissipative region, which indicates that all simulations are carried out with the good resolution at small scales. Although the slope of $\langle u_r^2 \rangle$ could be estimated for large Reynolds numbers as seen from Fig. 1, the scaling exponents of higher order structure functions as well as low order ones for small Reynolds numbers can be reliably evaluated only on the basis of the ESS method, i.e., by plotting $\langle u_r^p \rangle$ against $\langle u_r^3 \rangle$ [1–3].

In order to know the r dependence of $\zeta_p(r)$ for various Reynolds numbers, we prepare Fig. 2, in which $\zeta_p(r)$ with $p=4,6,8$ are depicted for $R_\lambda = 69,125,259,374$, and 459. (The eighth order structure function is confirmed to converge statistically.) Note that the data for scales larger than integral scales are not shown, because a universal property of turbulence is not expected in those data. It is remarkable that there is a dip at about $r/\eta \sim 10$, and that it grows in depth with increasing Reynolds number. The exception is the case $R_\lambda = 69$, where a dip does not appear. As the scale increases beyond the dip, $\zeta_4(r)$ and $\zeta_6(r)$ tend to approach constant values, although the corresponding data for $R_\lambda = 259$ behave in a slightly different way from other cases. For $p=8$ the

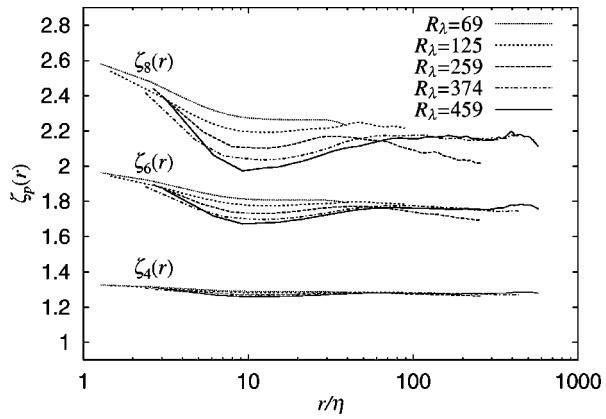

FIG. 2. The ELSS exponents $\zeta_4(r)$, $\zeta_6(r)$, and $\zeta_8(r)$ against r/η for various values of Reynolds number. The data with scales larger than integral scales are deleted from the figure.

situation is the same as for $p=6$, but the variation is larger. It is of interest to notice that for the largest Reynolds number 459 the flat region is observed in the interval $100 \lesssim r/\eta \lesssim 300$, which may be identified with the inertial region. For smaller Reynolds numbers it is a little difficult to find the flat region. For $R_\lambda = 69$ we see the flat region in the interval $10 \lesssim r/\eta \lesssim 30$, and the corresponding slopes for $p \geqslant 4$ are larger than those for $R_\lambda = 459$. However, the flat region at smaller scales for $R_\lambda = 69$ is different from one at larger scales for $R_\lambda = 459$.

Before we compare the formula (10) with the data, the validity of the log-normal distribution of the velocity increment should be ensured. The probability density function (PDF) of the intermediate amplitudes is certainly log normal. In order to determine the range of the log normality, we calculated a peak position $u_r^*(p)$ of $u_r^p P(u_r)$ at $r/\eta = 24$ for $R_\lambda = 121$. The PDF is satisfactorily fitted by a log-normal curve for $u_r^*(p=1.5) \leqslant u_r \leqslant u_r^*(p=6)$. On the other hand, the PDF of ε_r is found to be log normal in much wider interval. If we employ the same notation as above, the log normality of ε_r holds at least in the interval of $\varepsilon_r^*(p=-4) \leqslant \varepsilon_r \leqslant \varepsilon_r^*(p=6)$ for the same Reynolds number. If the refined similarity hypothesis $u_r^3 \sim r\varepsilon_r$ is assumed to hold for any amplitude, the corresponding PDF of u_r should be log normal for $u_r^*(p=-12) \leqslant u_r \leqslant u_r^*(p=18)$, which is much wider than the observed log-normal interval. The reason for the discrepancy is that the refined similarity holds only for the intermediate amplitudes of ε_r in agreement with the observation [15–17]. Hence, the use of the log-normal expression for the exponent (10) is completely justified for intermediate values of p.

In order to analyze a nature of the r dependence of the local slope $\zeta_p(r)$, we rewrite Eq. (10) in the following form:

$$\frac{\zeta_p}{p} = \left(\frac{1}{3} + \frac{\mu(r)}{6}\right) - \frac{\mu(r)}{18} p. \tag{12}$$

What is the range of p? To decide the range we calculated $\zeta_p(r)$ for various values of p at units of 0.1 at $r/\eta = 24$ for $R_\lambda = 121$, and plotted ζ_p/p against p. Although such a plot is not given here, ζ_p/p is fitted by a straight line for $1 \leqslant p \leqslant 6$. The curve is deviated upward from the straight fitting line for $p \geqslant 7$ and downward for $0 < p < 1$. Hence the comparison will be made in the range $1 \leqslant p \leqslant 6$, but the intermittency coefficient $\mu(r)$ estimated there plays a significant role to represent even the whole intermittency effect.

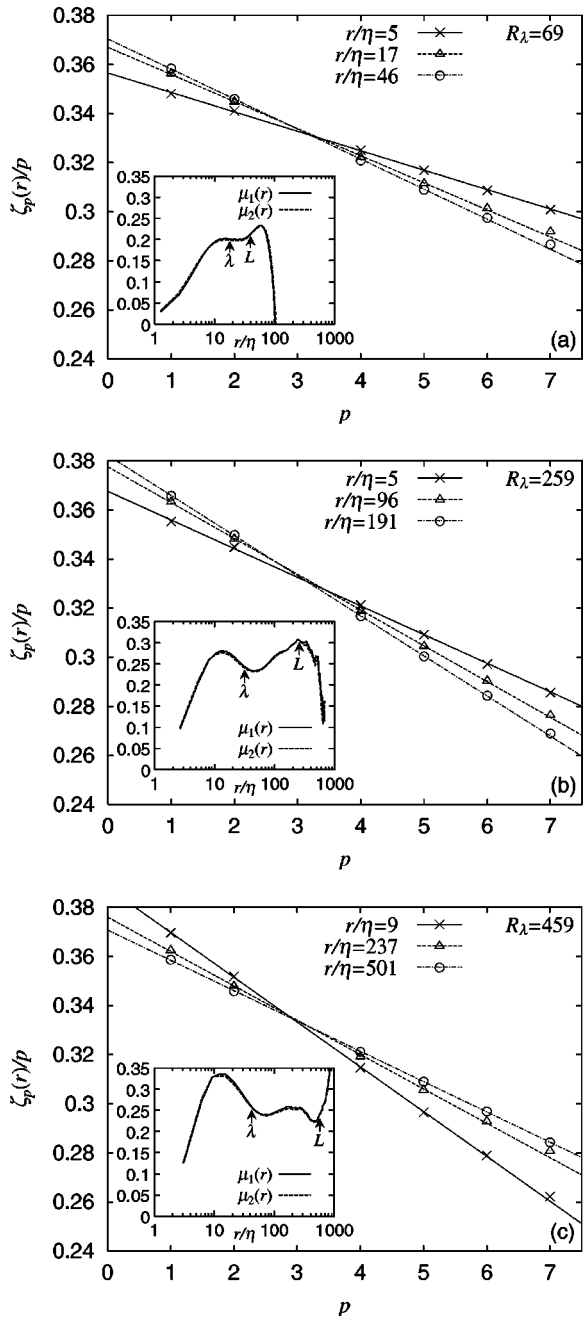

FIG. 3. The ELSS exponents $\zeta_p(r)/p$ against p obtained in the DNS for different values of r and for different Reynolds numbers; (a) $R_\lambda = 69$, (b) $R_\lambda = 259$, and (c) $R_\lambda = 459$. Straight lines, which are the best fit line for $1 \leqslant p \leqslant 6$, indicate agreement of the data with the representation (12). The inset shows local intermittency exponent $\mu(r)$ calculated using the data. $\mu_1(r)$ corresponds to calculations using the ''slope'' method (described in the text), and $\mu_2(r)$ does to those using the ''intersection'' method. Calculated Taylor length λ and the integral length L are marked for convenience.

Figure 3(a) shows a curve $\zeta_p(r)/p$ vs p for several values of r/η with $R_\lambda = 69$. Straight lines in this figure are the best fit lines for $1 \leqslant p \leqslant 6$. The data points for $p=7$, which are not included for the comparison, are slightly deviated from the log-normal lines as mentioned above. Intermittency index, $\mu(r)$, can be calculated from this figure using the slope of the fitting straight lines or the intersection point of the fitting straight lines with vertical axis [cf. Eq. (12)]. The calculated values of $\mu(r)$ are shown in the inset of the Fig. 3(a) (μ_1 corresponds to calculations using the ''slope'' method, whereas μ_2 are given by the ''intersection'' method.) In the plot of $\mu(r)$ Taylor microscale λ and an integral scale L are marked for convenience. (We have confirmed the well-known prediction [19] $\lambda/\eta = 15^{1/4} R_\lambda^{1/2}$ and $L/\eta \sim R_\lambda^{3/2}$.) For Reynolds numbers 259 and 459 we have obtained similar pictures (Figs. 3b and 3c). Other Reynolds numbers give the same result.

As seen from Figs. 3(a) to 3(c), $\mu(r)$ substantially depends on r with a typical ''two-maxima'' shape. Even for $R_\lambda = 69$ in Fig. 3(a) there is a small peak around $r/\eta \sim 10$. Local maximum of the $\mu(r)$ at smaller scales exhibits a few interesting properties. (I) For $R_\lambda = 50$ the maximum is not observed, and the first appearance of the maximum occurs at R_λ between 50 and 69. (II) A position of this maximum (normalized by η) is independent of Reynolds number, and takes value $\ell_1 \approx 14\eta$, which is actually the beginning of the dissipative region. (III) Value of $\mu(\ell_1)$ scales with R_λ as $\mu(\ell_1) \sim R_\lambda^{0.26}$. (IV) The scale λ is located on the right descending hill.

The flat region where $\mu(r)$ is constant appears in between $r/\eta \sim 100$ and $r/\eta \sim 300$ for the highest Reynolds number $R_\lambda = 459$ [see Fig. 3(c)]. In such an interval $\mu(r) \approx 0.25$. This value is consistent with those known in literature for observations corresponding to very large Reynolds number [20,21].

It should be noted that strong tubelike vortices are believed to be sparsely distributed in space in fully developed turbulence [9,22]. Those vortices are frequently assumed as Burgers' vortex with mean radius 10η [22]. The energy dissipation takes place strongly around those vortices. Therefore extreme intermittency of the energy dissipation at this scale is consistent with the observation of the maximum of $\mu(r)$ at scale $r = 14\eta$. On the other hand, the usual scaling region, where $\zeta_p(r)$ as well as $\mu(r)$ are independent of scale in a certain interval of scale, can be seen only for largest Reynolds number, $R_\lambda = 459$ in the present work. Such a scaling region is located for $r > \lambda$; in our simulation the scaling region starts from approximately 2.5λ.

T.G. was supported by a Grant-in Aid for Scientific Research (C-2) 12640118 from the Japan Society for the Promotion of Science. We are very grateful to RIKEN Computer Center and Nagoya University Computer Center for their support. T. Ochiai at NIT is also acknowledged for his assistance in numerical computation involved in this work. One of the authors, A.B., is grateful to C. H. Gibson and K. R. Sreenivasan for numerous discussions on the problem.

[1] R. Benzi, S. Ciliberto, R. Tripiccione, C. Baudet, F. Massailoli, S. Succi, Phys. Rev. E **48**, R29 (1993).
[2] R. Benzi, S. Ciliberto, C. Baudet, and G.R. Chavarria, Physica D **80**, 385 (1995).
[3] B. Dhruva, Y. Tsuji, and K.R. Sreenivasan, Phys. Rev. E **56**, R4928 (1997).
[4] K.R. Sreenivasan and B. Dhruva, Prog. Theor. Phys. Suppl. **130**, 103 (1998).
[5] N. Cao, S. Chen, and Z.-S. She, Phys. Rev. Lett. **76**, 3711 (1996).
[6] S. Grossmann, D. Lohse, and A. Reeh, Phys. Rev. E **56**, 5473 (1997).
[7] A. Bershadskii, Europhys. Lett. **39**, 587 (1997).
[8] D. Fukayama, T. Oyamada, T. Nakano, T. Gotoh, and K. Yamamoto, J. Phys. Soc. Jpn. **69**, 701 (2000).
[9] J. Jimenez and A.A. Wray, J. Fluid Mech. **373**, 255 (1998), related references therein.
[10] R.M. Kerr, M. Meneguzzi, and T. Gotoh, e-print physics/0005004.
[11] Z.-S. She and E. Leveque, Phys. Rev. Lett. **72**, 336 (1994).
[12] A.M. Oboukhov, J. Fluid Mech. **13**, 77 (1962).
[13] A.N. Kolmogorov, J. Fluid Mech. **13**, 82 (1962).
[14] A. S. Monin and A. M. Yaglom, *Statistical Fluid Mechanics* (MIT Press, Cambridge, 1975) Vol. 2.
[15] A. Praskovsky, Phys. Fluids A **4**, 2589 (1992).
[16] S.T. Thoroddsen and C.W. Van Atta, Phys. Fluids A **4**, 2592 (1992).
[17] G. Stolovitzky, P. Kailasnath, and K.R. Sreenivasan, Phys. Rev. Lett. **69**, 1178 (1992); See also G. Stolovitzky and K.R. Sreenivasan, Rev. Mod. Phys. **66**, 229 (1994) for the relation between the μ and ζ_p exponents.
[18] T. Gotoh and D. Fukayama, Phys. Rev. Lett. **86**, 3775 (2001).
[19] H. Tennekes and J.L. Lumley, *First Course in Turbulence* (MIT Press, Cambridge, 1972).
[20] K.R. Sreenivasan and P. Kailasnath, Phys. Fluids A **5**, 512 (1993).
[21] A. Praskovsky and S. Oncley, Phys. Fluids **6**, 2886 (1994).
[22] For instance, consult T. Miyauchi and M. Tanahashi, in *Proceedings of IUTAM Symposium on Geometry and Statistics of Turbulence*, edited by T. Kambe (Kluwer, Dordrecht, 2001), pp. 67–76.